Research Square

Preprints are preliminary reports that have not undergone peer review.
They should not be considered conclusive, used to inform clinical practice,
or referenced by the media as validated information.

Assessment of Digital Quasi-2D and 2.5D Micromodels for Pore-scale Two-phase Flow

Hyunjee Yoon

yyhj0302@snu.ac.kr

Seoul National University

Renato Poli

The University of Texas at Austin

Maša Prodanović

The University of Texas at Austin

Hoonyoung Jeong

Seoul National University

Research Article

Keywords: microfluidics, micromodel, lattice Boltzmann method, digital rock physics, 2.5D, multiphase, relative permeability

Posted Date: March 20th, 2026

DOI: https://doi.org/10.21203/rs.3.rs-9013820/v1

License: This work is licensed under a Creative Commons Attribution 4.0 International License.
Read Full License

Additional Declarations: No competing interests reported.

Assessment of Digital Quasi-2D and 2.5D Micromodels for Pore-scale Two-phase Flow

Hyunjee Yoon[1*], Renato Poli[2,3], Maša Prodanović[2*], Hoonyoung Jeong[1,4,5*]

[1]Department of Energy Systems Engineering, Seoul National University, 1, Gwanak-ro, Gwanak-gu, Seoul, 08826, Republic of Korea.
[2]Department of Petroleum and Geosystems Engineering, University of Texas at Austin, 2515 Speedway, Austin, 78712, Texas, United States.
[3]Petrobras, Rua Marquês de Herval 90, 11010-310, Santos, São Paulo, Brazil.
[4]Research Institute of Energy and Resources, Seoul National University, 1, Gwanak-ro, Gwanak-gu, Seoul, 08826, Republic of Korea.
[5]Seoul National University Energy Initiative, Seoul National University, 1, Gwanak-ro, Gwanak-gu, Seoul, 08826, Republic of Korea.

*Corresponding author(s). E-mail(s): yyhj0302@snu.ac.kr; masha@utexas.edu; hoonyoung.jeong@snu.ac.kr;
Contributing authors: rpoli@utexas.edu;

Abstract

Microfluidic experiments are widely used to visualize pore-scale multiphase flow, yet conventional quasi-2D micromodels often fail to capture three-dimensional (3D) flow mechanisms such as snap-off. Variable-depth 2.5D micromodels can address this limitation experimentally, but their numerical accuracy in predicting transport properties remains unquantified. In this study, we developed a computational workflow to generate digital quasi-2D and 2.5D micromodels and quantify their performances. Five geometric parameters of *slice index*, *erosion radius*, *thickness*, *slope*, and *cross-section geometry* are introduced to adjust the model geometries. The generated digital micromodels are evaluated using two-phase lattice Boltzmann method (LBM) simulations. By comparing relative permeability curves and fluid configurations against a 3D reference

model, we demonstrate that the digital 2.5D micromodel outperforms the digital quasi-2D micromodel. The digital 2.5D micromodel yielded an RMSE ten times lower (0.013) than that of the quasi-2D micromodel (0.132). Sensitivity analysis identified *erosion radius* as the most influential parameter and a symmetric cross-sectional geometry as a better cross-section geometry. We also provide recommended values for geometric parameters based on the pore and throat size statistics. This workflow can also serve as a valuable screening tool for micromodel geometry optimization prior to physical fabrication.

Keywords: microfluidics, micromodel, lattice Boltzmann method, digital rock physics, 2.5D, multiphase, relative permeability

1 Introduction

The characterization of multiphase fluid flow through porous media is fundamental to applications in geoscience and engineering, including hydrocarbon recovery, carbon sequestration, and groundwater management (Blunt 2017). Microfluidic experiments have been used to understand how fluid/fluid displacement occurs in porous media (Karadimitriou and Hassanizadeh 2012; Du et al. 2021; Wang et al. 2022) since their introduction in the 1950s (Chatenever and Calhoun 1952). Microfluidic experiments utilize micromodels to visualize pore-scale displacement processes by using transparent materials such as glass with an etched geometry of arbitrary, image-based complexity that can be observed with a microscope.

The most common type of micromodels are conventional uniform-depth (quasi-2D) micromodels. However, the quasi-2D micromodels often fail to replicate 3D trapping phenomena such as snap-off (Anbari et al. 2018; Xu et al. 2017).

To overcome the limitation of quasi-2D micromodels, Xu et al. (2017) proposed a 2.5D micromodel. The etching depth of the 2.5D micromodel varies spatially to create a more topographically representative pore space. This design successfully replicated complex multiphase flow behaviors in physiscal experiments, particularly the snap-off phenomenon. With this advantage of 2.5D micromodels, they were used in multiple enhanced oil recovery studies (Wang et al. 2022; Mejia et al. 2019).

However, current studies (Xu et al. 2017; Anbari et al. 2018; Du et al. 2021; Wang et al. 2022; Lei et al. 2025) focus primarily on experimental observations, leaving the numerical accuracy of 2.5D geometries in predicting transport properties such as relative permeability largely unquantified.

Numerical performance of a digital micromodel can be evaluated using digital rock physics (DRP) workflow. DRP has emerged as an effective tool to link pore-scale geometry to core- and field-scale transport properties (Blunt 2017). DRP typically involves acquiring three-dimensional (3D) images of rock samples (Figure 1) using X-ray micro-computed tomography (μCT) (Blunt et al. 2013; Wildenschild and Sheppard 2013) and subsequently performing direct numerical simulations on the digitized pore space. Direct numerical simulations calculate the transport properties of fluid flow in porous media by solving the governing equations.

Lattice Boltzmann method (LBM) is one of the widely used tools for pore scale flow analysis (Pan et al. 2006; Maier and Bernard 2010; Porter et al. 2012). LBM simulates flow directly from pore geometries and provide detailed velocity and pressure fields that are difficult to obtain experimentally. LBM also allows the modeling of complex multiphysics, including multiphase flow, reactive transport, and heat transfer (Ginzburg 2007; Kang et al. 2006, 2010; Liu et al. 2013; Landry and Karpyn 2012; Landry et al. 2016).

In this study, we present a workflow to generate digital quasi-2D and 2.5D micromodels and compare their performance using LBM multiphase simulation. We introduce five geometric parameters to adjust the model geometries: *slice index*, *erosion radius*, *slope*, *thickness*, and *cross-section geometry*. In particular, *cross-section geometry* is introduced to better represent the converging-diverging structure of natural porous media. These parameters allow for additional image processing on the digital micromodels that cannot be easily controlled in physical micromodel fabrication.

Additionally, this digital workflow can be used to screen micromodel geometries before the actual microfluidic experiments. By digitally testing and filtering different structures prior to physical fabrication, researchers can avoid trial-and-error and save significant time and costs.

We generate the digital 2.5D micromodels as well as the digital quasi-2D micromodels, from cross-sections of a 3D digital rock image. We then perform two-phase LBM flow simulation and compare the resulting relative permeability curves and residual oil distributions with those obtained from the full 3D simulation. Here, we chose relative permeability as an important transport property in porous media, but a similar workflow can be applied to other properties. Finally, a sensitivity analysis is performed with the geometric parameters of the digital quasi-2D and 2.5D micromodels (hereafter, quasi-2D and 2.5D models) to understand their impact on the numerical performance.

2 Methodology

The methodology of this study is divided into three main stages: (1) generation of digital quasi-2D and 2.5D micromodels (hereafter, quasi-2D and 2.5D models) from a digital 3D reference model, (2) pore-scale flow simulations for relative permeability calculation, and (3) post-processing using the Brooks-Corey model for error analysis. Each stage is described in detail below.

2.1 Model generation workflow

In this study, two types of digital model were employed: quasi-2D and 2.5D models. Quasi-2D models were generated by extruding a selected 2D cross-section from a 3D image. For 2.5D models, the approach of (Xu et al. 2017) was used, where pores and throats are assigned different depths. Unlike the regular patterns employed by Xu et al. (2017), we employed a more realistic sand pack image (Figure 1) for both quasi-2D and 2.5D models.

The generation of the quasi-2D and 2.5D models is governed by five geometric parameters: *slice index*, *erosion radius*, and *thickness* for both modes, additionally *slope* and *cross-section geometry* for 2.5D models. While both models are inspired by physical micromodels, these parameters introduce additional geometric degrees of freedom beyond what is achievable in physical micromodel fabrication. The python workflow can be found on GitHub (Yoon 2026). The specific role of each parameter is described in the following paragraphs.

The quasi-2D and 2.5D model generation workflow is divided into what we refer to as horizontal (within a slice of data) and vertical (adding depth) processing. Horizontal processing involves slice selection, morphological erosion, and connected component analysis to avoid numerical instability in simulation. First, a 2D cross-section is selected from a full 3D reference model (Figure 1) based on *slice index*. Because individual 2D slices often lack the connectivity of the 3D reference model, morphological erosion is applied to the grain pixels to widen the pore space. Morphological erosion is a non-linear image processing operation that shrinks the foreground objects (grains) by peeling away layers of pixels from the object boundaries. The magnitude of the enlargement of the pore space by this operation is controlled by *erosion radius* of a disk-shaped element. As shown in Figure 2, increasing *erosion radius* expands the pore space and ensures percolation. Next, the connected component analysis identifies the main flow path and isolated pore clusters. Because isolated pore clusters do not contribute to flow and can cause numerical instability in simulation, they are removed and converted to grain pixels (Figure 3).

Vertical processing adds depth using *thickness*, *slope*, and *cross-section geometry* to the 2D image. The process begins by extruding the 2D image to a specified *thickness*. For quasi-2D models, a uniform depth is assigned to the entire pore space. For 2.5D models, an additional etching process is applied to the pore space.

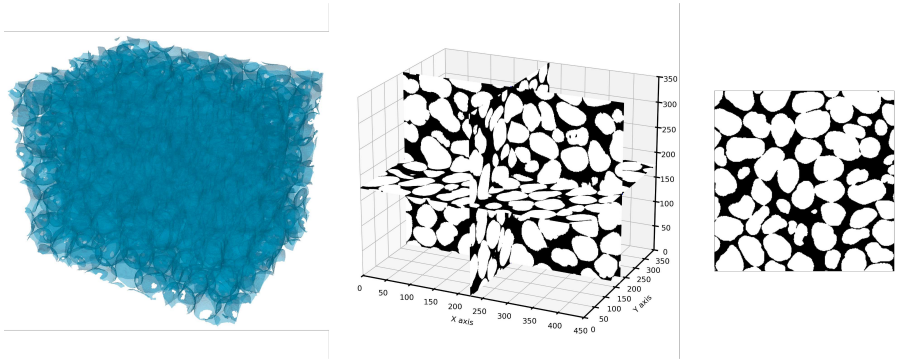
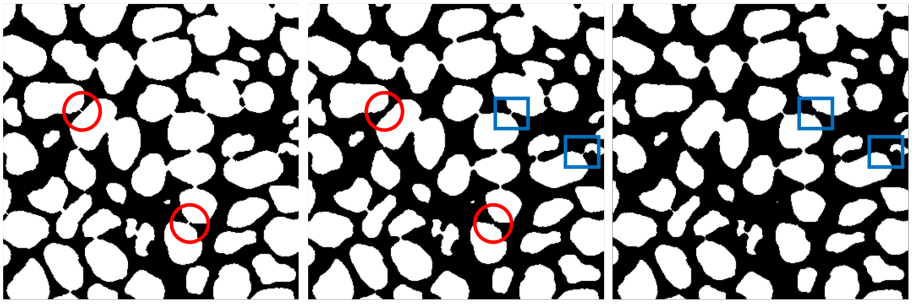


Fig. 1: Visualization of the 3D reference sand pack model: 3D isosurface (left), internal cross-section view (middle), and a 2D cross-sectional image from the 3D model (right).



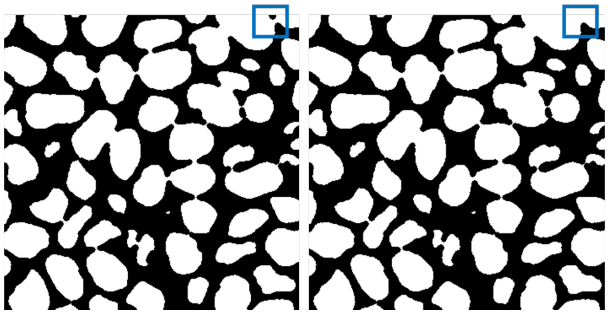
(a) Erosion radius of 2 (b) Erosion radius of 3 (c) Erosion radius of 4

Fig. 2: Comparison of pore connectivity after morphological erosion using different erosion radius of (a) 2, (b) 3, and (c) 4. Red circles (radius 2 $\rightarrow$ 3) and blue squares (radius 3 $\rightarrow$ 4) shows that the flow paths are opened with larger radius.

The etching depths are calculated using a distance map and *slope*. Distance map represents the distance to the nearest grain voxel Figure 4. The *slope* parameter controls the gradient of the etched surface and is expressed as:

$$Slope = \frac{h(x,y)}{d(x,y)} \tag{1}$$

where $h(x,y)$ is the assigned depth of the pore and $d(x,y)$ is the Euclidean distance from the voxel at (x,y) to the nearest grain. A larger *slope* generates a steeper etched



(a) Before (b) After

Fig. 3: Comparison of the pore structure (a) before and (b) after connected component analysis. The blue square highlights isolated pore clusters that are disconnected from the main flow path and subsequently removed.

surface. As *slope* approaches infinity, the 2.5D geometry converges to that of a quasi-2D model (Figure 5). Thus, *slope* allows for a continuous transition between quasi-2D and 2.5D.

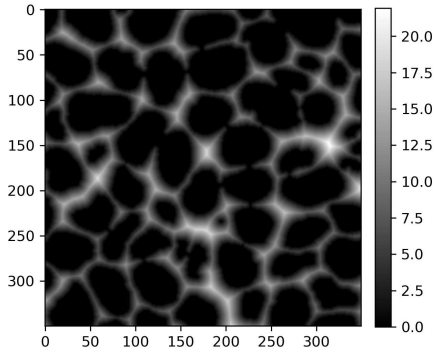


Fig. 4: Distance map of a representative slice. Each value of a voxel represents the distance between the voxel and the nearest grain voxel.

We also introduce *cross-section geometry* for the vertical processing. Typically, physical 2.5D models have a shape that the pore is widest at the top and narrowest at the bottom. However, we introduce a *symmetric* cross-section geometry that the pore is etched outward from the central plane to better represent the converging-diverging topology of pores (Figure 6).

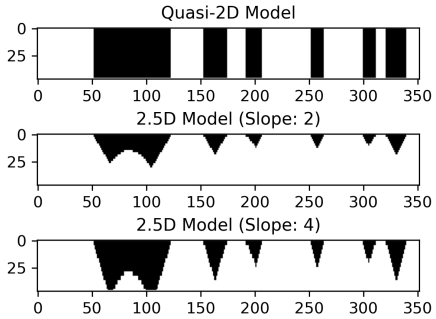


Fig. 5: Comparison of cross-section of quasi-2D and 2.5D models for different *slope* values. As *slope* increases, the pore space (black) deepens, creating steeper grain boundaries (white). As *slope* approaches infinity, the geometry converges to a quasi-2D model.

Finally, the *cross-section geometry* defines the shape of the etching. Physical 2.5D micromodels typically have an asymmetric cross-section geometry where the pore is widest at the top and narrows toward the bottom. In this digital workflow, however, we introduce a *symmetric* cross-section geometry. With the symmetric cross-section geometry, the pore space is etched outward from the central plane so that it can better represent the converging-diverging topology of natural porous media (Figure 6).

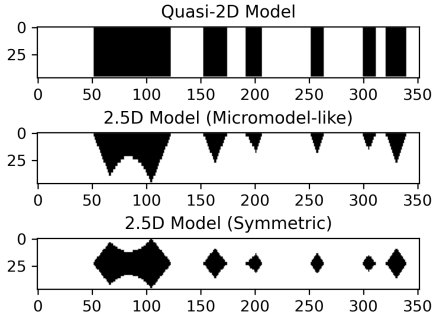


Fig. 6: Comparison of cross-sections for different *cross-section geometry*. Top: Uniform depth profile of the quasi-2D model. Middle: 2.5D model with asymmetric, *micromodel-like* cross-section (depth increases from top to bottom). Bottom: 2.5D model with *symmetric* cross-section (depth increases outward from the central plane).

2.2 Numerical Modeling

2.3 Lattice Boltzmann simulations

We employed the lattice Boltzmann method (LBM) for the direct pore-scale two-phase simulation (Latva-Kokko and Rothman 2005; Armstrong et al. 2016) of the models. Simulations were performed using the open-source lattice Boltzmann methods for porous media (LBPM) package within the open porous media (OPM) project (McClure et al. 2021; Flemisch et al. 2021).

The simulation workflow consists of two major steps: morphological drainage and multiphase flow simulation. The morphological drainage initializes the model saturation to a preset value based on the morphology of the pore space that water occupies the tightest pore throats. We used the one implemented in LBPM (McClure et al. 2021).

After the initialization with morphological drainage, the multiphase flow simulation estimates the relative permeability using the fractional flow protocol of the color model. The fractional flow protocol estimates the relative permeability in steady state. From the initial fluid configuration of water saturation of approximately 10%, the water saturation is increased and stabilized until the capillary number converges. After the capillary number converges, the outputs are registered, and the water saturation is increased again until the endpoint.

The fluid properties used for the simulation are summarized in Table 1. The relaxation time (τ) of the fluids is associated with the viscosity as $\mu = \frac{1}{3}\left(\tau - \frac{1}{2}\right)$ (Pan et al. 2006). The capillary number is the ratio of viscous force to capillary force, given by $Ca = \frac{\mu v}{\sigma}$, where μ is the fluid viscosity, v is modulus of the fluid velocity and σ is the fluid-fluid interfacial tension (McClure et al. 2021).

2.4 Post-processing

The performance of the quasi-2D and 2.5D models was evaluated using two outputs from numerical simulation: relative permeability curves and the fluid configuration at the end of imbibition.

To quantify the similarity between the relative permeability curves, the root mean square error (RMSE) was used as the primary evaluation metric. However, calculating a direct point-by-point error from the raw simulation data presents two challenges. First, the raw LBM outputs from different models do not align at the exact same saturation intervals. Second, the relative permeability curves of the 3D, quasi-2D, and 2.5D models are defined over different saturation ranges due to varying initial water (S_{wi}) and residual oil (S_{or}) saturations.

To address these issues and ensure a robust comparison, we processed the raw data with the following steps. First, the simulation results were fitted to the Brooks-Corey correlation to make the relative permeability curves continuous:

$$k_{rw} = k_{rw,max} S_{w,eff}^{N_w} \tag{2}$$

$$k_{ro} = k_{ro,max} (1.0 - S_{w,eff})^{N_o} \tag{3}$$

where $k_{rw,max}$ and $k_{ro,max}$ are the endpoint relative permeability values, and N_w and N_o are the Corey exponents for water and oil, respectively. The effective water saturation, $S_{w,eff}$, is normalized using the initial water saturation (S_{wi}) and residual oil saturation (S_{or}):

$$S_{w,eff} = \frac{S_w - S_{wi}}{1 - S_{wi} - S_{or}} \tag{4}$$

The optimal Corey exponents (N_w, N_o) were determined through non-linear least-squares optimization using an automated Python framework.

Next, we mapped all curves onto a common x-axis ranging from 0 to 1 using effective water saturation to ensure a consistent comparison of the curves. Then,

RMSE relative to the 3D reference curves was calculated on the common x-axis as a quantifying metric of the performance of the digital micromodels:

$$RMSE = \sqrt{\frac{1}{N}\sum_{i=1}^{N}\left(k_r^i - k_{r,3D}^i\right)^2} \tag{5}$$

where N is the total number of saturation points on the normalized $S_{w,eff}$ axis, and $k_r^{(i)}$ and $k_{r,3D}^{(i)}$ represent the relative permeabilities of the digital micromodel and the 3D reference model at the i-th point, respectively.

Additionally, for the sensitivity analysis, the relative errors of the individual Brooks-Corey fitting parameters were evaluated to quantify their deviation from the 3D reference model. The relative error is calculated as:

$$Relative\ error\ (\%) = \left|\frac{P - P_{3D}}{P_{3D}}\right| \times 100 \tag{6}$$

where P is the specific fitting parameter value (S_{or}, $k_{rw,max}$, N_o, or N_w) derived from the digital micromodel, and P_{3D} is the corresponding ground-truth value obtained from the 3D reference model.

Fluid configuration at the end of imbibition can be visualized by highlighting the oil phase in red color (Figure 10). At the end of imbibition, water has highest relative permeability whereas oil loses its ability to flow. Therefore, all the oil phase at the end of imbibition can be considered as snap-off at the residual oil saturation, S_{or}. This allows for a direct qualitative comparison of the oil trapping mechanisms among the different model geometries.

3 Results

In this section, we first present the results of the 3D model as a ground truth. We then compare the base cases of the quasi-2D and 2.5D models against these 3D results.

Finally, we present a sensitivity analysis to demonstrate how the input parameters affect the accuracy of the quasi-2D and 2.5D models.

3.1 3D Reference Model

As a 3D reference model, we use a high-resolution micro-computed tomography (μCT) image of a uniform quartz sand pack from a silver nano-particle injection experiment (Prodanovic et al. 2025; Turhan et al. 2024; Molnar 2016). The 3D image has a voxel length of 9.87 μm and dimensions of 450 $\times$350$\times$350 voxels. The grayscale image is segmented using Otsu's thresholding method (Otsu 1979), resulting in a model with a porosity of 43% and absolute permeability of 320 mD.

The pore and throat size distributions calculated from the extracted network of the 3D reference model are shown in Figure 7. Pore and throat equivalent diameter means the area equivalent circle's diameter. Here, we identified the percentile of both the pore diameter and throat diameter to use as a *erosion radius* and *thickness*. For this specific image, the P50 of pore diameter and the P30 of throat diameter are 9 voxels (89 μm) and 3 voxels (30 μm), respectively.

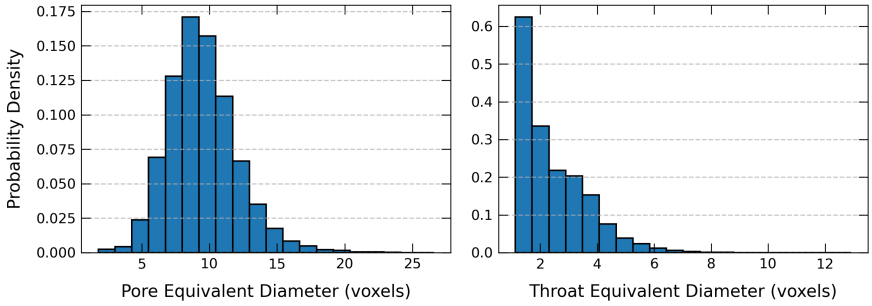


Fig. 7: Pore size distribution and throat size distribution of the 3D reference model.

We employed the fractional flow protocol of the color model to simulate a two-phase water-oil system, as detailed in Table 1. The simulation used unity ratios for fluid density and viscosity and assumed a strongly water-wet condition consistent with

the quartz medium. We configured the inlet and outlet with five mixing layers each to ensure stable boundary conditions. Furthermore, we selected a small capillary number of 10^{-4} to ensure a capillary-dominated flow regime.

The two-phase flow properties were simulated using a steady-state fractional flow protocol within the open source software Lattice Boltzmann in Porous Media (LBPM). For the morphological drainage process, the model was initialized to an initial water saturation (S_{wi}) of 10%, which approximates the fluid configuration after a primary drainage process. Then, for the multi-phase flow simulation process, the water saturation is increased in discrete steps. Once a steady state was achieved, the water fractional flow was increased to produce a target saturation increment of 5% for the next steady point. The simulation terminates when the non-wetting phase (oil) flow rate drops below 10% of the total flow rate, as determined by the endpoint threshold value which indicates residual oil saturation has been reached.

Table 1: Parameters for multiphase LBPM simulations.

Parameter	Value	Description
P_c	10^{-4}	Capillary number
α	0.005	Controls the interfacial tension $\sigma = 6\alpha$
τ	0.7	Relaxation parameter related to the viscosity of the fluids
F_b	10^{-5} N	Body force (downwards, z-direction)

3.2 Base cases of quasi-2D and 2.5D

The base cases for the quasi-2D and 2.5D models were generated using the parameters listed in Table 2. A representative slice (b, the 51st slice) from the 3D model shown in Figure 1 was used for both models. An *erosion radius* of 3 (P30 of throat diameter probability distribution) and a *thickness* of 45 voxels (10% of the original 3D model's depth, 5 times of P50 of pore diameter probability distribution) were used. For the 2.5D

model, two additional parameters were defined: *slope* was set to 3 (about 72 °), and a symmetric cross-section geometry was employed for the base case. These parameters were selected without calibrating and further sensitivity analysis on these parameters is presented in the subsequent subsection.

Table 2: Base case parameters for quasi-2D and 2.5D models.

Parameter	Quasi-2D model	2.5D model
Slice index	b (51)	
Erosion radius [voxels]	3 (≃ P30 of pore diameter)	
Thickness [voxels]	45 (≃ 5× P50 of pore diameter)	
Slope	–	3 (≃ 72 °)
Cross-section geometry	–	Symmetric

The pore size and throat size distributions of the quasi-2D and 2.5D base case models with the 3D reference are shown in Figure 8. The distributions from the 2.5D model were a closer match to the 3D model than the quasi-2D model for both pore size and throat size distrubutions.

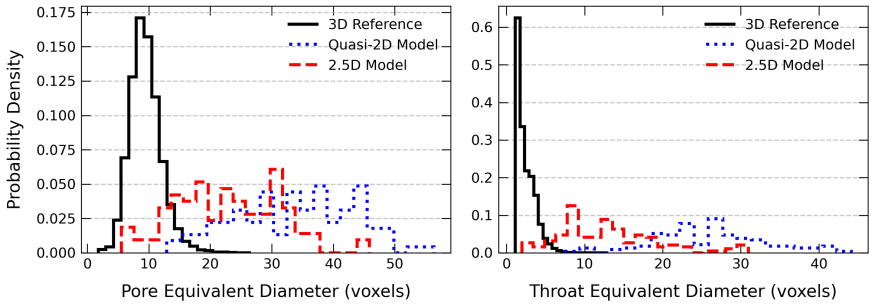


Fig. 8: Pore size (left) and throat size (right) distributions of the quasi-2D (blue dotted line) and 2.5D (red dashed line) base case models. The 3D reference model is plotted with black solid lines.

Multiphase flow simulation was performed on the digital quasi-2D and 2.5D models using the LBPM. We used the input parameters identical to the 3D reference model (Table 1).

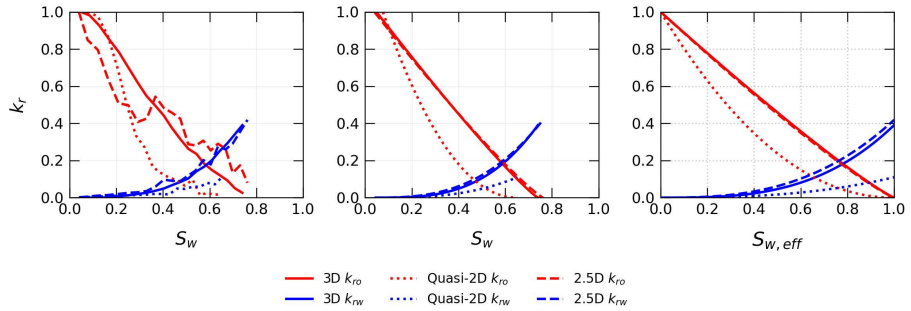


Fig. 9: Comparison of relative permeability curves for the 3D reference, quasi-2D, and 2.5D models. Left to right: raw simulation data, Brooks-Corey fitted curves, and normalized curves on effective saturation values. Solid, dotted, and dashed lines represent the 3D, quasi-2D, and 2.5D models, respectively.

Figure 9 compares the relative permeability results of the digital micromodels against the 3D reference model. The 2.5D model showed a significantly higher accuracy than the quasi-2D model. While the raw simulation data of the 2.5D model for the oil phase (shown in red) exhibits some numerical oscillations, the Brooks-Corey fitted curves demonstrate that the 2.5D model nearly perfectly replicates the 3D ground truth for both the wetting and non-wetting phases. In contrast, the quasi-2D model underestimates the overall relative permeability for both oil and water.

The performance difference between quasi-2D and 2.5D models can also be observed in Table 3. The 2.5D model achieved an exceptional RMSE of 0.013, which ten times lower than the RMSE of the quasi-2D model of 0.132.

The visual distribution of the residual oil also shows this performance differences (Figure 10). We can see the 2.5D model shows the snap-off, as in the experiments (Xu et al. 2017). On the other hand, the oil blobs of quasi-2D model were notably

Table 3: The Brooks-Corey fitting parameters and RMSE of the relative permeability curves of the quasi-2D and 2.5D models against the 3D reference model.

Parameter	3D Reference model	Quasi-2D model		2.5D model	
	Value	Value	Relative Error(%)	Value	Relative Error(%)
S_{or}	0.26	0.35	34.62	0.24	7.69
$k_{rw,max}$	0.39	0.11	72.79	0.42	7.69
N_o	1.12	2.07	84.82	1.15	2.68
N_w	3.09	2.71	12.30	2.76	10.68
RMSE	-	0.132		0.013	

larger and connected over multiple pores, which results in the overestimation of S_{or} (Table 3).

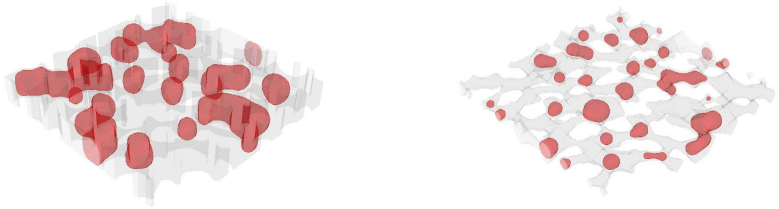


Fig. 10: Fluid configuration of quasi-2D (left) and 2.5D (right) models at the end of imbibition. The red blobs represent the remaining oil blobs.

3.3 Sensitivity Analysis

To further investigate the influence of the geometric parameters used in model generation, a sensitivity analysis was performed on the RMSE between curves and the prediction errors of the Brooks-Corey fitting parameters. First, by varying the geometric parameters one at a time, we evaluated how the RMSE of the sensitivity cases

deviates from the base case using Equation (5). The design of the sensitivity analysis is summarized in Table 4.

Table 4: Sensitivity analysis design for quasi-2D and 2.5D models. Categorical slice indices are labeled a, b, and c. Numeric parameters are varied by approximately ± 30% from the base case.

		Sensitivity Analysis Cases	
Parameter	Base Case	Low	High
Slice index	b (51)	a (47)	c (56)
Erosion radius	3	2(-33%)	4(+33%)
Thickness	45	32(-30%)	59(+30%)
Slope	3	2(-33%)	4(+33%)
Cross-section geometry	Symmetric	Micromodel-like	

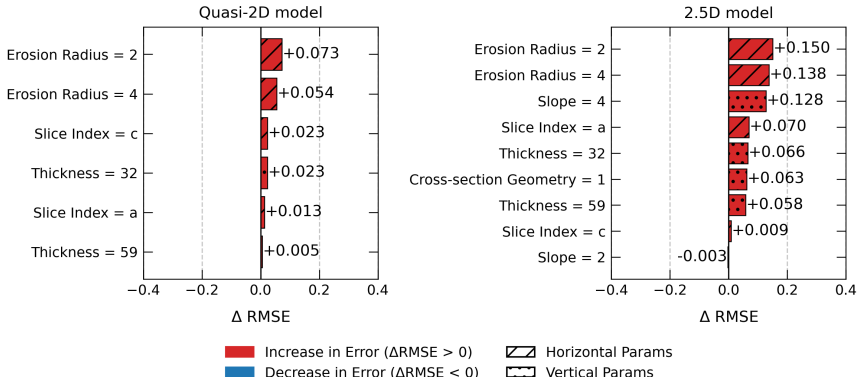


Fig. 11: Windsock plots illustrating the sensitivity of the root mean square error (RMSE) of the relative permeability curves for the quasi-2D (left) and 2.5D (right) models compared to the 3D reference. Red and blue bars indicate an increase and decrease in RMSE relative to the base case, respectively. Hatched and dotted patterns represent horizontal parameters (*slice index*, *erosion radius*) and vertical parameters (*thickness*, *slope*, and *cross-section geometry*), respectively. For the cross-section geometry, 0 value represents the micromodel-like geometry.

First, the overall impact of each geometric parameter was assessed using a windsock plot sorted by sensitivity (Figure 11). For both the quasi-2D and 2.5D models,

erosion radius was the most influential parameter. This result shows the critical need to establish appropriate flow paths, as both quasi-2D and 2.5D models inherently lack the pore connectivity of the original 3D structure. As shown in Figure 2, the flow paths are closed with the smaller radius and thus interfere with the fluid flow. In the same way, if the flow paths are opened too much, the original pore geometry can be lost.

In Figure 11, the quasi-2D model was predominantly affected by horizontal parameters (slice index and radius), while the 2.5D model showed a balanced sensitivity to both horizontal and vertical parameters (slope and cross-section geometry). This indicates that the additional adjustment of the depth profile of the 2.5D model can add more degree of freedom in optimizing the micromodel performance.

Next, we plotted the variation in the relative error of the individual Brooks-Corey fitting parameters as the geometric parameter changes from base case to sensitivity cases. We calculated the relative error between each Brooks-Corey fitting parameters of quasi-2D or 2.5D model and the 3D model using Equation (6).

First, the impact of *erosion radius* is studied. *Erosion radius* is a parameter used for morphological opening, which expands the pore space to ensure fluid pathways are connected. A larger *erosion radius* increases porosity and makes it easier for fluid to flow by widening both pores and throats (Figure 2). This effect is especially important for creating or enlarging narrow throats that might otherwise block flow.

In Figure 12, we can see *erosion radius* of 3 worked well with this specific sample. Since *erosion radius* was the most influential parameter, the value must be carefully optimized. For the 2.5D model, the P30 of throat equivalent diameter worked the best, and this is recommended as a practical starting point when optimizing the micromodel geometry.

Next, the effect of *slice index* is studied. *Slice index* is a categorical variable that determines which cross-section from the 3D image to be used to build the quasi-2D and 2.5D models. *Slice index* is a critical parameter because it defines the entire pore

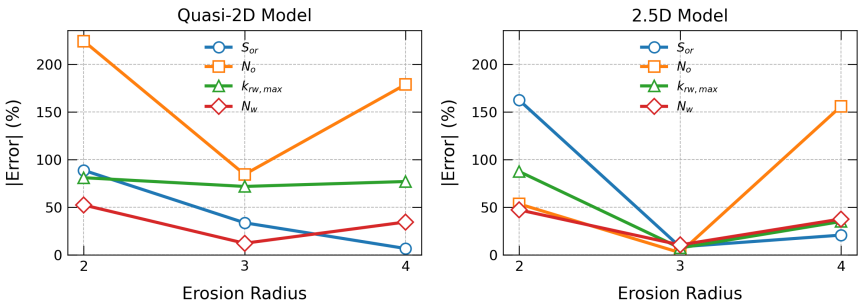


Fig. 12: Sensitivity of relative error of Brooks-Corey parameters to *erosion radius* for the quasi-2D (left) and the 2.5D (right) models. Relative errors of Brooks-Corey parameters are compared against the 3D reference for different *erosion radius* values. The x- and y-axes represent *erosion radius* and the relative error to 3D reference model, respectively.

structure for the model. Although adjacent slices may be similar, the index number itself does not have numerical meaning. For this analysis, we used the 51st slice as the base case and also tested the 46th and 56th slices (referred to as slices a, b, and c).

Figure 13 shows the changes in individual fitting parameters when *slice index* changes. With the varying *slice index*, the 2.5D model showed a lower error variability compared to the quasi-2D model across all selected slices. For highly heterogeneous rocks where slice selection is critical, this workflow can serve as a numerical screening tool to find a representative slice.

Thickness determines the thickness of the micromodels and also the maximum depth the pore can have. Figure 14 shows the effect of *thickness* on the fitting parameters. Similar to slice index, the 2.5D model showed a lower error variability compared to the quasi-2D model. This again suggests that the model parameters should be optimized for the best results.

Slope is a parameter that defines the steepness of the 2.5D model. As *slope* increases, the pore space becomes wider and steeper. Therefore, theoretically, a 2.5D model with an infinite *slope* is equivalent to a quasi-2D model (Figure 5). Our results

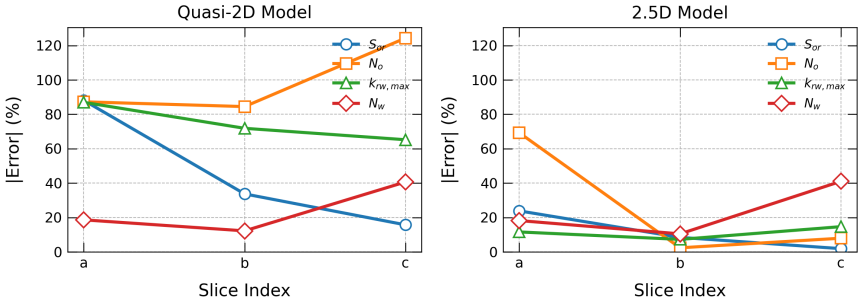


Fig. 13: Sensitivity of relative error of Brooks-Corey parameters to *slice index* for the quasi-2D (left) and the 2.5D (right) models. Relative errors of Brooks-Corey parameters are compared against the 3D reference for different *slice index* values. The x- and y-axes represent *slice index* and the relative error to 3D reference model, respectively.

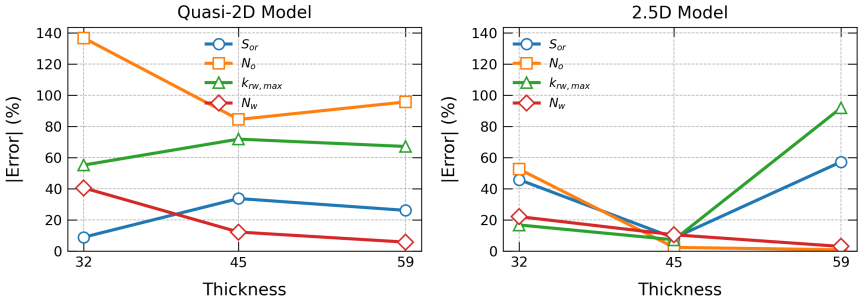


Fig. 14: Sensitivity of relative error of Brooks-Corey parameters to *thickness* for the quasi-2D (left) and the 2.5D (right) models. Relative errors of Brooks-Corey parameters are compared against the 3D reference for different *thickness* values. The x- and y-axes represent *thickness* and the relative error to 3D reference model, respectively.

showed that the prediction error increased as *slope* increases (Figure 15). This finding supports our main conclusion that the 2.5D model is superior to the quasi-2D model.

Notably, the error of N_o was significantly lower in the 2.5D model compared to the quasi-2D model in the sensitivity results of all three parameters.

Cross-section geometry is a categorical variable that determines how the 2.5D vertical structure is generated. The options were symmetric (etched from the center outwards) or micromodel-like (etched from the top down). When we changed the geometry from symmetric to micromodel-like, the prediction error for all fitting parameters

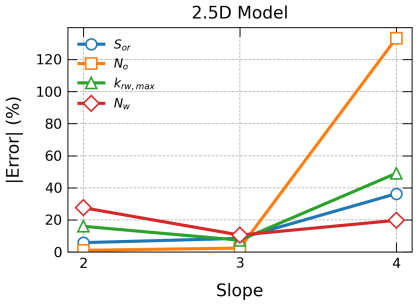


Fig. 15: Sensitivity of relative error of Brooks-Corey parameters to *slope* for the 2.5D model. Relative errors of Brooks-Corey parameters are compared against the 3D reference for different *slope* values. The x- and y-axes represent *slope* and the relative error to 3D reference model, respectively.

increased (Figure 16). This indicates that the symmetric geometry provides a more accurate representation of the 3D pore space.

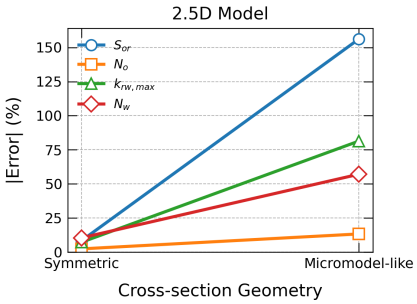


Fig. 16: Sensitivity of relative error of Brooks-Corey parameters to *cross-section geometry* for the 2.5D model. Relative errors of Brooks-Corey parameters are compared against the 3D reference for different *cross-section geometry* value. The x- and y-axes represent the *cross-section geometry* and the relative error, respectively.

4 Conclusion

In this study, we developed a workflow to generate digital quasi-2D and 2.5D micromodels and to evaluate their numerical performance in terms of relative permeability using two-phase lattice Boltzmann method simulations.. The results demonstrate that

the 2.5D model significantly outperforms the quasi-2D model in predicting relative permeability curves and fluid configurations of the 3D reference model. The 2.5D model successfully reproduced relative permeability curves with the root mean squared error (RMSE) of 0.013, ten times lower than the quasi-2D model of 0.132. From the sensitivity analysis on the RMSE, *erosion radius* was identified as the most influential parameter for both the quasi-2D and the 2.5D models. Notably, while the quasi-2D model was dominantly influenced by horizontal parameters, the 2.5D model was influenced by both horizontal and vertical parameters. This confirms that the additional degrees of freedom provided by the 2,5D configuration are useful to create a more representative digital micromodel. Furthermore, we found that a symmetric cross-section geometry yields better agreement with 3D model than the traditional micromodel-like profile by better representing the converging-diverging geometry of pore. From a practical standpoint, we found that using the P30 of the throat diameter for *erosion radius* and 5 times the P50 of the pore diameter for *thickness* proved effective for the specific sandpack model. These values can serve as a recommended starting point for parameter selection. This proposed workflow can also serve as a screening tool to optimize the micromodel geometries and select the optimal slice prior to physical fabrication to save time and resources. Future work should focus on validating this methodology on more complex, heterogeneous rock types and under various wettability conditions to broaden its applicability.

Supplementary information. Not applicable.

Acknowledgements. The authors acknowledge the Texas Advanced Computing Center (TACC) at The University of Texas at Austin for providing computational resources that have contributed to the research results reported within this paper. URL: http://www.tacc.utexas.edu

Declarations

Funding

Financial support for Hyunjee Yoon was provided by Korea Environment Industry & Technology Institute (KEITI) through National R&D Program on Integrated Management Technologies for Global Carbon Regulations funded by Korea Ministry of Environment (MOE) [Grant ID: RS-2025-02213131] which is carried out by the GHG Reduction Potential Assessment Consortium based on the Technology Database for Carbon Neutrality, and the Institute for Korea Spent Nuclear Fuel (iKSNF) and National Research Foundation of Korea(NRF) grant funded by the Korea government(Ministry of Science and ICT, MSIT) [Grant ID: 2021M2E1A108519422].

Financial support for Renato Poli was provided by Petrobras (Petróleo Brasileiro S.A.) through a PhD fellowship.

Competing Interests

The authors declare no competing interests.

Ethics approval

Not applicable.

Consent for publication

Not applicable.

Data availability

The study utilized publicly available data from the Digital Porous Media Portal (formerly Digital Rocks Portal) (Molnar 2016).

Materials availability

Not applicable.

Code availability

The image processing workflow developed to modify the Digital Porous Media Portal data is available on GitHub (Yoon 2026) at https://digitalporousmedia.org/.

Author Contributions

- **H. Yoon**: Conceptualization, Methodology (Proxy model generation), Software (Python workflow development), Writing – original draft & editing, Visualization (Figures 1–16).
- **R. Poli**: Conceptualization, Methodology (Numerical modeling), Software (LBPM simulation setup), Investigation (Running high-performance LBM simulations), Writing – review & editing.
- **M. Prodanović**: Conceptualization, Resources, Project administration, Supervision, Writing – review & editing.
- **H. Jeong**: Supervision, Funding acquisition, Writing – review & editing.

If any of the sections are not relevant to your manuscript, please include the heading and write 'Not applicable' for that section.

References

Anbari A, Chien HT, Datta SS, et al (2018) Microfluidic Model Porous Media: Fabrication and Applications. Small 14(18):1703575. https://doi.org/10.1002/smll.201703575

Armstrong RT, McClure JE, Berrill MA, et al (2016) Beyond Darcy's law: The role of phase topology and ganglion dynamics for two-fluid flow. Physical Review E 94(4):043113. https://doi.org/10.1103/PhysRevE.94.043113

Blunt MJ (2017) Multiphase Flow in Permeable Media, 1st edn. Cambridge University Press, West Nyack

Blunt MJ, Bijeljic B, Dong H, et al (2013) Pore-scale imaging and modelling. Advances in Water Resources 51:197–216. https://doi.org/10.1016/j.advwatres.2012.03.003

Chatenever A, Calhoun JCJr. (1952) Visual Examinations of Fluid Behavior in Porous Media - Part I. Journal of Petroleum Technology 4(06):149–156. https://doi.org/10.2118/135-G

Du Y, Xu K, Mejia L, et al (2021) A Coreflood-on-a-Chip Study of Viscoelasticity's Effect on Reducing Residual Saturation in Porous Media. Water Resources Research 57(8):e2021WR029688. https://doi.org/10.1029/2021WR029688

Flemisch B, Flornes K, Lie KA, et al (2021) OPM: The Open Porous Media Initiative. URL https://www.researchgate.net/publication/258463298_OPM_The_Open_Porous_Media_Initiative

Ginzburg I (2007) Lattice Boltzmann modeling with discontinuous collision components: Hydrodynamic and Advection-Diffusion Equations. Journal of Statistical Physics 126(1):157–206. https://doi.org/10.1007/s10955-006-9234-4

Kang Q, Lichtner PC, Zhang D (2006) Lattice Boltzmann pore-scale model for multicomponent reactive transport in porous media. Journal of Geophysical Research: Solid Earth 111(B5):2005JB003951. https://doi.org/10.1029/2005JB003951

Kang Q, Lichtner PC, Viswanathan HS, et al (2010) Pore Scale Modeling of Reactive Transport Involved in Geologic CO2 Sequestration. Transport in Porous Media 82(1):197–213. https://doi.org/10.1007/s11242-009-9443-9

Karadimitriou NK, Hassanizadeh SM (2012) A Review of Micromodels and Their Use in Two-Phase Flow Studies. Vadose Zone Journal 11(3):vzj2011.0072. https://doi.org/10.2136/vzj2011.0072

Landry CJ, Karpyn ZT (2012) Single-phase lattice Boltzmann simulations of pore-scale flow in fractured permeable media. International Journal of Oil, Gas and Coal Technology 5(2/3):182. https://doi.org/10.1504/IJOGCT.2012.046320

Landry CJ, Prodanović M, Eichhubl P (2016) Direct simulation of supercritical gas flow in complex nanoporous media and prediction of apparent permeability. International Journal of Coal Geology 159:120–134. https://doi.org/10.1016/j.coal.2016.03.015

Latva-Kokko M, Rothman DH (2005) Diffusion properties of gradient-based lattice Boltzmann models of immiscible fluids. Physical Review E 71(5):056702. https://doi.org/10.1103/PhysRevE.71.056702

Lei W, Gong W, Lu X, et al (2025) 3-D-geometry-triggered transition from monotonic to non-monotonic effects of wettability on multiphase displacements in homogeneous porous media. Journal of Fluid Mechanics 1014:R2. https://doi.org/10.1017/jfm.2025.10196

Liu H, Valocchi AJ, Zhang Y, et al (2013) Phase-field-based lattice Boltzmann finite-difference model for simulating thermocapillary flows. Physical Review E 87(1):013010. https://doi.org/10.1103/PhysRevE.87.013010

Maier R, Bernard R (2010) Lattice-Boltzmann accuracy in pore-scale flow simulation. Journal of Computational Physics 229(2):233–255. https://doi.org/10.1016/j.jcp.2009.09.013

McClure JE, Li Z, Berrill M, et al (2021) The LBPM software package for simulating multiphase flow on digital images of porous rocks. Computational Geosciences 25(3):871–895. https://doi.org/10.1007/s10596-020-10028-9

Mejia L, Tagavifar M, Xu K, et al (2019) Surfactant flooding in oil-wet micromodels with high permeability fractures. Fuel 241:1117–1128. https://doi.org/10.1016/j.fuel.2018.12.076

Molnar I (2016) Uniform quartz - Silver nanoparticle injection experiment [Dataset]. Digital Porous Media Portal. https://doi.org/10.17612/P7Z59J

Otsu N (1979) A Threshold Selection Method from Gray-Level Histograms. IEEE Transactions on Systems, Man, and Cybernetics 9(1):62–66. https://doi.org/10.1109/TSMC.1979.4310076

Pan C, Luo LS, Miller CT (2006) An evaluation of lattice Boltzmann schemes for porous medium flow simulation. Computers & Fluids 35(8-9):898–909. https://doi.org/10.1016/j.compfluid.2005.03.008

Porter ML, Coon ET, Kang Q, et al (2012) Multicomponent interparticle-potential lattice Boltzmann model for fluids with large viscosity ratios. Physical Review E 86(3):036701. https://doi.org/10.1103/PhysRevE.86.036701

Prodanovic M, Esteva M, Ketcham R, et al (2025) Digital Porous Media Portal (DPMP) for Publication, Analysis, and Simulation of Porous Media Images. https://doi.org/doi.org/10.17612/FGMN-D889

Turhan C, Chang B, Mohamed A, et al (2024) Digital Porous Media Portal for Image Curation, Characterization, Visualization, and Transport Simulation in Porous Media. p 1056, URL https://jgmaas.com/SCA/2024/SCA2024_1056.pdf

Wang N, Liu Y, Cha L, et al (2022) Experimental Investigation of Trapped Oil Mobilization with Ferrofluid. SPE Journal 27(01):753–770. https://doi.org/10.2118/201365-PA

Wildenschild D, Sheppard AP (2013) X-ray imaging and analysis techniques for quantifying pore-scale structure and processes in subsurface porous medium systems. Advances in Water Resources 51:217–246. https://doi.org/10.1016/j.advwatres.2012.07.018

Xu K, Liang T, Zhu P, et al (2017) A 2.5-D glass micromodel for investigation of multi-phase flow in porous media. Lab on a Chip 17(4):640–646. https://doi.org/10.1039/C6LC01476C

Yoon H (2026) 2.5D-Model/2p5d_proxy_generation_workflow.ipynb at main · HyunjeeYoon/2.5D-Model. URL https://github.com/HyunjeeYoon/2.5D-Model/blob/main/2p5d_proxy_generation_workflow.ipynb